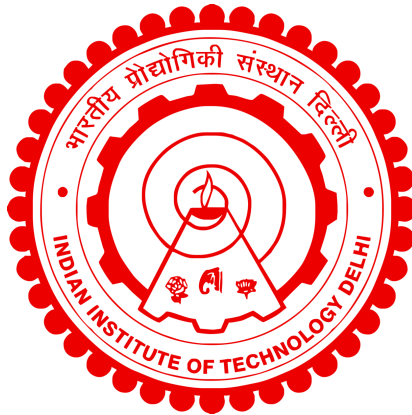


LINEAR STABILITY OF NON-NEWTONIAN FLUID FLOWS

SUBHAM PAL



DEPARTMENT OF APPLIED MECHANICS

INDIAN INSTITUTE OF TECHNOLOGY DELHI

August 2023

© Indian Institute of Technology Delhi (IITD), New Delhi, 2023

LINEAR STABILITY OF NON-NEWTONIAN FLUID FLOWS

by

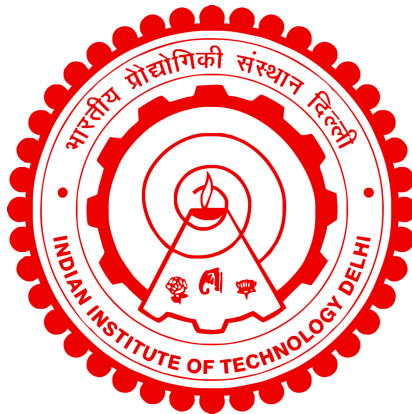
SUBHAM PAL

Department of Applied Mechanics

Submitted

in fulfillment of the requirements of the degree of Doctor of Philosophy

to the



**INDIAN INSTITUTE OF TECHNOLOGY
DELHI**

August 2023

Certificate

This is to certify that the thesis **Mr. Subham Pal** submitted for consideration for the degree of Doctor of Philosophy at the Indian Institute of Technology Delhi, entitled "**Linear Stability of Non-Newtonian Fluid Flows**" is an accurate account of the legitimate research work he conducted under my direction and supervision. I believe that the thesis is deserving of consideration for the degree of Doctor of Philosophy under Institute regulations as **Mr. Subham Pal** has complied with all the necessary prerequisites. The contents of this thesis have not been submitted in whole or in part to any other college or institute for the granting of any degree or diploma.

Dr. Arghya Samanta

Associate Professor
Department of Applied Mechanics
Indian Institute of Technology Delhi
New Delhi-110016
India

Place: New Delhi

Date :

Acknowledgements

Ph.D is more than a degree, it's a total package for enthusiastic people who dreams to research on various delicate as well as interesting topics of nature, society as well as industries. During this period I experienced both easy and difficult times, but through out the period I enjoyed and appreciated all the things that happened across me. Definitely it is not something I achieved on my own, but the collective support of various individuals which always driven me to move forward in the positive direction.

First of all I would like to thank my supervisor Prof. Arghya Samanta for taking me under his wing. He was the first person who introduced me to this field of 'Hydrodynamic Stability'. He guided me with very much care to be a detail-oriented, qualified, and creative researcher. He was more than a supervisor, a friend, and also a guardian during my stay in the institute. He is an independent researcher and the huge amount of research work he is doing every year is always amazing. The way he works, sacrificing almost all the social enjoyments is truly tough to achieve. He allowed all his lab students to visit him any time, even on the weekends for research discussion. Honestly speaking, he is so workaholic that I dared to give him any excuse for any of my negligence. All these things influenced me toward a very positive direction and ultimately helped to reach to this point, for which I will be always in debt to him.

The members of my Student Research Committee, I would like to thank Prof. S.V. Veeravalli, Prof. A. Bhattacharya, and Prof. P.P. Chokshi for their insightful remarks and ideas during the study process. The course "Transport Phenomenon of Complex Fluids" by Prof. Chokshi helped me get a better understanding of the viscoelastic liquid models and polymer mechanism, which helped me in getting the clear picture of things happening in the viscoelastic stability problems.

I consider myself really lucky to have a senior, Dr. Farooq Ahmed Bhat, who guided me to be more thorough and precise with the numerical simulation. He helped me with some short yet beautiful advices whenever I asked him any of my doubts. I am glad to have friends like Satyam, Shrey, Parveen, Abhay, Sandeep, Puneet, Abhimanyu, and Prakhar who made my stay in IIT Delhi fun. And my two football-buddies Kabir and Utplendu, thank you for all the positive vibes. Furthermore, I

would like thank my lab mates and colleagues who helped me explicitly or implicitly during this period.

Last but not least, I owe my parents, Mr. Subhash Chandra Pal and Mrs. Sipra Paul, my sincere gratitude and admiration for continuous support, blessings, and inspiration throughout my life. I am really lucky to have them, in fact they understood me the best and gave full support toward my dream to become a researcher of science. The way my father handled everything at home, and my mother who supported him with the cause, helped me to concentrate properly in my work and gave me courage to keep standing against all odds. I will always be grateful to them since I needed it the most.

Subham Pal

Abstract

In general, the falling film instability at the surface of a viscous liquid occurs under the action of gravitational force, where the surface wave propagates downstream through a sequence of nonlinear events and, finally, leads to a large tear-drop shape solitary wave. Since then there have been many studies on the stability of Newtonian liquids. The studies of viscoelastic liquid flows have piqued the interest of many researchers because of their vast technological and medical field applications. For example, the coating technology industries have long relied on viscoelastic liquids for their various rheological properties. Furthermore, viscoelastic liquids can be added for improving the performance of multigrade oils used as a lubricant in loaded journal bearings. In addition, investigation of such liquids is very fruitful in understanding the liquid lining flows in pulmonary airways. In this thesis, we tried to investigate different viscoelastic liquid models under different flow conditions.

In the first study, a linear stability analysis of a surfactant-laden viscoelastic liquid flowing down a slippery inclined plane is carried out under the framework of Orr-Sommerfeld-type eigenvalue problem. It is assumed that the viscoelastic liquid satisfies the rheological property of Walters' liquid B'' . The Orr-Sommerfeld-type eigenvalue problem is solved analytically and numerically based on the long-wave analysis and Chebyshev spectral collocation method, respectively. The long-wave analysis predicts the existence of two temporal modes, the so-called surface mode and surfactant mode, where the first-order temporal growth rate for the surfactant mode is zero. However, the first-order temporal growth rate for the surface mode is non-zero, which leads to the critical Reynolds number for the surface mode. Furthermore, it is found that Re_c for the surface mode reduces with the increasing value of the viscoelastic coefficient and ensures a destabilizing effect of the viscoelastic coefficient on the primary instability induced by the surface mode in the long-wave regime. On the other hand, the numerical result demonstrates that the viscoelastic coefficient has a non-trivial stabilizing influence on the surface mode when the Reynolds number is far away from the onset of instability. Furthermore, if the Reynolds number is high and the inclination angle is sufficiently low, there exists another mode, namely the shear mode. The unstable region induced by the shear mode magnifies significantly even for the weak effect of the viscoelastic coefficient

and makes the transition faster from stable to unstable flow configuration for the viscoelastic liquid. Moreover, the slip length exhibits a dual role in the surface mode as reported for the Newtonian liquid. But it exhibits only a stabilizing effect on the shear mode. In addition, it is found that the Marangoni number also exhibits a dual nature on the primary instability induced by the surface mode in contrast to the result of the Newtonian liquid.

In the second study, a linear stability analysis is carried out for a contaminated viscoelastic liquid flowing down an inclined plane when there was an externally applied shear stress at the liquid surface, where the elastic behaviour of the liquid follows the upper-convected Maxwell (UCM) model. The earlier work [H. H. Wei, “Stability of a viscoelastic falling film with surfactant subjected to an interfacial shear,” *Phys. Rev. E* **71**, 066306 (2005)] conducted analytically in the long-wave regime is revisited again in exploring the results in the arbitrary wavenumber regime. An Orr-Sommerfeld-type eigenvalue problem is formed for the viscoelastic liquid and solved both analytically and numerically by using the long-wave expansion and Chebyshev spectral collocation technique, respectively. It is found that with the increase in the value of the Weissenberg number, the critical Reynolds number for the surface mode reduces, but the stable region enhances in the finite wavenumber regime. Furthermore, the unstable domain induced by the surface mode reduces in the presence of insoluble surfactant but enhances in the presence of applied shear stress. If the Reynolds number is high, but the inclination angle is small, the shear mode arises in the numerical simulation, which becomes weaker in the presence of the Marangoni number but becomes stronger in the presence of the Weissenberg number and applied shear stress. In a special case, it is demonstrated that the present study recovers the results of Walters’ liquid B'' in the limit of the low viscoelastic parameter.

In the third part of the study, we investigate a linear stability analysis for the Oldroyd-B liquid draining down a slippery inclined plane where a constant shear stress is applied at the liquid surface in the streamwise direction. The aim is to expand the previous study [E. S. G. Shaqfeh, R. G. Larson, and G. H. Fredrickson, “The stability of gravity driven viscoelastic film-flow at low to moderate Reynolds number,” *J. Non-Newtonian Fluid Mech.* **31**, 87 (1989)] in the presence of imposed shear stress when the bounding plane is slippery. The stability analysis is executed

analytically as well as numerically for low to high values of the Reynolds number, which detects the existence of surface and shear modes. In the low Reynolds number regime, we use the analytical long-wave asymptotic expansion to find the onset of primary instability for the surface mode. On the other hand, we implement the numerical Chebyshev spectral collocation technique to determine the short-wave instability when the Reynolds number changes from a moderate to a high value. It is found that the critical Reynolds number for the surface mode decreases with the increasing values of the slip length and imposed shear stress, and thereby, the surface instability occurs at a lower Reynolds number than that when the slip length and the imposed shear stress are excluded. More specifically, the imposed shear stress has a destabilizing effect on the surface mode when acting in the co-flow direction but a stabilizing effect when acting in the counter-flow direction. Furthermore, the viscosity ratio exhibits a stabilizing influence on the surface mode near the onset of instability but exhibits a destabilizing effect far away from the onset of instability. In the high Reynolds number regime, the primary instability induced by the shear mode is stabilized by increasing the viscosity ratio and slip length, but can be destabilized by applying a constant shear stress in the co-flow direction. In a special case, the result for the surface mode corresponding to Walters' liquid B'' can be recovered from that of the Oldroyd-B liquid if the viscoelastic parameter is kept at a very low value.

For the fourth study, we take a case of horizontal channel flow of a weakly viscoelastic liquid that follows the constitutive model of Walters' liquid B'' . A linear stability analysis is performed when the channel walls are slippery. In this case, the viscoelastic channel flow is driven by the streamwise pressure-gradient. We explore the primary instability for a symmetric slip flow with the same slip length of the channel walls, an asymmetric slip flow with different slip lengths of the channel walls, and an analogy to the Poiseuille-Couette flow of a viscoelastic liquid with a slip effect on the lower wall but no slip effect on the upper wall. We observe that the viscoelastic parameter shows a destabilizing impact, but the slip length shows a stabilizing impact on the most unstable shear mode in all three flow configurations. Moreover, the Poiseuille and Poiseuille-Couette flows for the viscoelastic liquid are linearly more unstable to infinitesimal disturbances than those of the Newtonian liquid. As a result, wall velocity needs to be higher than in the Newtonian liquid to stabilize the

viscoelastic Poiseuille-Couette flow. Using the asymptotic analysis, we have determined the critical value of the slip length, or equivalently, the critical value of the lower wall velocity, above which the asymmetric slip flow and the Poiseuille-Couette flow of the viscoelastic liquid are permanently stable to infinitesimal disturbances.

सारांश

सामान्य तौर पर, एक श्यान द्रव की सतह पर गिरती हुई फिल्म की अस्थिरता गुरुत्वाकर्षण बल की कार्रवाई के तहत होती है, जहां सतह की लहर गैर-रेखीय घटनाओं के अनुक्रम के माध्यम से नीचे की ओर फैलती है और अंत में, एक बड़े आंसू-बूंद आकार की एकान्त लहर की ओर ले जाती है। तब से न्यूटोनियन द्रव पदार्थों की स्थिरता पर कई अध्ययन हुए हैं। श्यान प्रत्यास्थ द्रव प्रवाह के अध्ययन ने इसके विशाल तकनीकी और चिकित्सा क्षेत्र के अनुप्रयोगों के कारण कई शोधकर्ताओं की रुचि बढ़ा दी है। उदाहरण के लिए, कोटिंग प्रौद्योगिकी उद्योग लंबे समय से अपने विभिन्न रियोलॉजिकल गुणों के लिए श्यान प्रत्यास्थ द्रव पदार्थों पर निर्भर रहे हैं। इसके अलावा, लोडेड जर्नल बियरिंग्स में स्नेहक के रूप में उपयोग किए जाने वाले मल्टीग्रेड तेलों के प्रदर्शन में सुधार के लिए श्यान प्रत्यास्थ द्रव पदार्थ जोड़े जा सकते हैं। इसके अलावा, फुफ्फुसीय वायुमार्ग में द्रव अस्तर के प्रवाह को समझने में ऐसे द्रव पदार्थों की जांच बहुत उपयोगी है। इस थीसिस में, हमने विभिन्न प्रवाह स्थितियों के तहत विभिन्न श्यान प्रत्यास्थ द्रव मॉडल की जांच करने का प्रयास किया।

पहले अध्ययन में, एक फिसलन वाले झुकाव वाले सतह से नीचे बहने वाले श्यान द्रव जिसमें अत्यधिक मात्रा में पृष्ठसक्रियक मिला हुआ है, का एक रैखिक स्थिरता विश्लेषण ऑर-सोमरफेल्ड-प्रकार के आइगेनवैल्यू समस्या के ढांचे के तहत किया जाता है। यह माना जाता है कि श्यान प्रत्यास्थ द्रव वाल्टर्स लिक्विड बी" की रियोलॉजिकल संपत्ति को संतुष्ट करता है। ऑर-सोमरफेल्ड-प्रकार की आइगेनवैल्यू समस्या को क्रमशः लंबी-तरंग विश्लेषण और चेबीशेव वर्णक्रमीय सह-स्थान विधि के आधार पर विश्लेषणात्मक और संख्यात्मक रूप से हल किया जाता है। लंबी-तरंग विश्लेषण दो अस्थायी प्रवाह, तथाकथित सतह प्रवाह और पृष्ठसक्रियक प्रवाह के अस्तित्व की भविष्यवाणी करता है, जहां सर्फैक्टेंट प्रवाह के लिए प्रथम-क्रम अस्थायी वृद्धि दर शून्य है। हालाँकि, सतह प्रवाह के लिए प्रथम-क्रम अस्थायी वृद्धि दर गैर-शून्य है, जो सतह प्रवाह के लिए महत्वपूर्ण रेनॉल्ड्स संख्या की ओर ले जाती है। इसके अलावा, यह पाया गया है कि सतह प्रवाह के लिए Re_c श्यान प्रत्यास्थ गुणांक के बढ़ते मूल्य के साथ कम हो जाता है और लंबी-तरंग क्षेत्र में सतह प्रवाह द्वारा प्रेरित प्राथमिक अस्थिरता पर श्यान प्रत्यास्थ सह-कुशल का एक अस्थिर प्रभाव सुनिश्चित करता है। दूसरी ओर, संख्यात्मक परिणाम दर्शाता है कि श्यान प्रत्यास्थ गुणांक का सतह प्रवाह पर एक गैर-तुच्छ स्थिरीकरण प्रभाव होता है जब रेनॉल्ड्स संख्या अस्थिरता की शुरुआत से बहुत दूर होती है। इसके अलावा, यदि रेनॉल्ड्स संख्या अधिक है और झुकाव कोण पर्याप्त रूप से कम है, तो एक और प्रवाह मौजूद है, अर्थात् अपरूपण प्रवाह। अपरूपण प्रवाह से प्रेरित अस्थिर क्षेत्र श्यान प्रत्यास्थ गुणांक के कमजोर प्रभाव के लिए भी काफी बढ़ जाता है और श्यान प्रत्यास्थ द्रव के लिए स्थिर से अस्थिर प्रवाह विन्यास में संक्रमण को तेज बनाता है। इसके अलावा, जैसा कि न्यूटोनियन द्रव के लिए रिपोर्ट किया गया है, स्लिप की लंबाई सतह प्रवाह में दोहरी भूमिका प्रदर्शित करती है। लेकिन यह केवल अपरूपण प्रवाह पर एक स्थिर प्रभाव प्रदर्शित करता है। इसके अलावा, यह पाया गया है कि मारंगोनी संख्या न्यूटोनियन द्रव के परिणाम के विपरीत सतह प्रवाह से प्रेरित प्राथमिक अस्थिरता पर दोहरी प्रकृति भी प्रदर्शित करती है।

दूसरे अध्ययन में, एक झुके हुए सतह से नीचे बहने वाले संदूषित श्यान प्रत्यास्थ द्रव के लिए एक रैखिक स्थिरता विश्लेषण किया जाता है, जब द्रव सतह पर बाहरी रूप से लागू अपरूपण तनाव होता है, जहां द्रव का श्यान व्यवहार ऊपरी-संवहन मैक्सवेल (UCM) मॉडल का अनुसरण करता है। पहले का काम [एच. एच. वेई, "एक इंटरफेशियल अपरूपण के अधीन पृष्ठसक्रियक के साथ एक श्यान प्रत्यास्थ गिरने वाली फिल्म की स्थिरता," फिजिकल रेव. ई **७१**, ०६६३०६ (२००५)] को लंबी-तरंग क्षेत्र में विश्लेषणात्मक रूप से किया गया है और मनमाने तरंग संख्या क्षेत्र में परिणामों की खोज में इसे फिर से दोहराया गया है। श्यान द्रव के लिए एक ऑर-सोमरफेल्ड-प्रकार की आइगेनवैल्यू समस्या बनाई गई है और क्रमशः लंबी-तरंग विस्तार और चेबीशेव वर्णक्रमीय संयोजन तकनीक का उपयोग करके विश्लेषणात्मक और संख्यात्मक रूप से हल किया गया है। यह पाया गया है कि वीसेनबर्ग संख्या के मूल्य में वृद्धि के साथ, सतह प्रवाह के लिए महत्वपूर्ण रेनॉल्ड्स संख्या कम हो जाती है, लेकिन स्थिर क्षेत्र परिमित तरंग संख्या क्षेत्र में बढ़ जाता है। इसके अलावा, सतह प्रवाह से प्रेरित अस्थिर प्रवाह क्षेत्र अघुलनशील पृष्ठसक्रियक की उपस्थिति में कम हो जाता है लेकिन लागू अपरूपण तनाव की उपस्थिति में बढ़ जाता है। यदि रेनॉल्ड्स संख्या अधिक है, लेकिन झुकाव कोण छोटा है, तो संख्यात्मक सिमुलेशन में

अपरूपण प्रवाह उत्पन्न होता है, जो मारंगोनी संख्या की उपस्थिति में कमजोर हो जाता है लेकिन वीसेनबर्ग संख्या और लागू अपरूपण तनाव की उपस्थिति में मजबूत हो जाता है। एक विशेष मामले में, यह प्रदर्शित किया गया है कि वर्तमान अध्ययन कम श्यान पैरामीटर की सीमा में वाल्टर्स लिक्विड बी के परिणामों को पुनर्प्राप्त करता है।

अध्ययन के तीसरे भाग में, हम एक फिसलन वाले झुकाव वाले सतह से नीचे बहने वाले ओल्ड्रॉयड-बी द्रव के लिए एक रैखिक स्थिरता विश्लेषण की जांच करते हैं, जहां धारा की दिशा में द्रव सतह पर एक निरंतर अपरूपण तनाव लागू होता है। इसका उद्देश्य पिछले अध्ययन का विस्तार करना है [ई. एस. जी. शक्फ्रेह, आर. जी. लार्सन, और जी. एच. फ्रेड्रिकसन, "निम्न से मध्यम रेनॉल्ड्स संख्या पर गुरुत्वाकर्षण संचालित श्यान प्रत्यास्थ फिल्म-प्रवाह की स्थिरता," जे. नॉन-न्यूटोनियन फ्लूइड मेक. **३१, ८७ (१९८९)**] जब बाउंडिंग सतह फिसलन भरा होता है तो लगाए गए अपरूपण तनाव की उपस्थिति में। स्थिरता विश्लेषण को रेनॉल्ड्स संख्या के निम्न से उच्च मूल्यों के लिए विश्लेषणात्मक और साथ ही संख्यात्मक रूप से निष्पादित किया जाता है, जो सतह और अपरूपण प्रवाह के अस्तित्व का पता लगाता है। कम रेनॉल्ड्स संख्या क्षेत्र में, हम सतह प्रवाह के लिए प्राथमिक अस्थिरता की शुरुआत का पता लगाने के लिए विश्लेषणात्मक लंबी-तरंग स्पर्शोन्मुख विस्तार का उपयोग करते हैं। दूसरी ओर, जब रेनॉल्ड्स संख्या मध्यम से उच्च मान में बदलती है तो हम शॉर्ट-वेव अस्थिरता को निर्धारित करने के लिए संख्यात्मक चेबीशेव वर्णक्रमीय संयोजन तकनीक लागू करते हैं। यह पाया गया है कि सतह प्रवाह के लिए महत्वपूर्ण रेनॉल्ड्स संख्या स्लिप लंबाई और लगाए गए अपरूपण तनाव के बढ़ते मूल्यों के साथ घट जाती है, और इस प्रकार, सतह अस्थिरता कम रेनॉल्ड्स संख्या पर होती है जब स्लिप लंबाई और लगाए गए अपरूपण तनाव होते हैं छोड़ा गया। अधिक विशेष रूप से, सह-प्रवाह दिशा में कार्य करते समय लगाया गया अपरूपण तनाव सतह प्रवाह पर एक अस्थिर प्रभाव डालता है, लेकिन प्रति-प्रवाह दिशा में कार्य करते समय एक स्थिर प्रभाव डालता है। इसके अलावा, श्यानता अनुपात अस्थिरता की शुरुआत के निकट सतह प्रवाह पर एक स्थिर प्रभाव प्रदर्शित करता है लेकिन अस्थिरता की शुरुआत से दूर एक अस्थिर प्रभाव प्रदर्शित करता है। उच्च रेनॉल्ड्स संख्या क्षेत्र में, अपरूपण प्रवाह से प्रेरित प्राथमिक अस्थिरता को श्यानता अनुपात और स्लिप लंबाई में वृद्धि करके स्थिर किया जाता है, लेकिन सह-प्रवाह दिशा में निरंतर अपरूपण तनाव लागू करके इसे अस्थिर किया जा सकता है। एक विशेष मामले में, यदि श्यान प्रत्यास्थ पैरामीटर को बहुत कम मूल्य पर रखा जाता है, तो वाल्टर्स लिक्विड बी के अनुरूप सतह प्रवाह का परिणाम ओल्ड्रॉयड-बी द्रव से पुनर्प्राप्त किया जा सकता है।

चौथे अध्ययन के लिए, हम एक कम श्यान द्रव के क्षैतिज चैनल प्रवाह का मामला लेते हैं जो वाल्टर्स लिक्विड बी के संवैधानिक मॉडल का अनुसरण करता है। जब चैनल की दीवारें फिसलन भरी होती हैं तो एक रैखिक स्थिरता विश्लेषण किया जाता है। इस मामले में, श्यान प्रत्यास्थ चैनल प्रवाह स्ट्रीमवाइज दबाव ढाल द्वारा संचालित होता है। हम चैनल की दीवारों की समान स्लिप लंबाई के साथ एक सममित स्लिप प्रवाह के लिए प्राथमिक अस्थिरता का पता लगाते हैं, चैनल की दीवारों की अलग-अलग स्लिप लंबाई के साथ एक असममित स्लिप प्रवाह, और एक श्यान प्रत्यास्थ द्रव के पॉइजुइल-कूएट प्रवाह के सादृश्य का पता लगाते हैं। निचली दीवार पर फिसलन का प्रभाव है लेकिन ऊपरी दीवार पर कोई फिसलन का प्रभाव नहीं है। हम देखते हैं कि श्यान प्रत्यास्थ पैरामीटर एक अस्थिर प्रभाव दिखाता है, लेकिन स्लिप लंबाई सभी तीन प्रवाह विन्यासों में सबसे अस्थिर अपरूपण प्रवाह पर एक स्थिर प्रभाव दिखाती है। इसके अलावा, श्यान प्रत्यास्थ द्रव के लिए पॉइजुइल और पॉइजुइल-कूएट प्रवाह न्यूटोनियन द्रव की तुलना में असीम छेड़छाड़ के लिए रैखिक रूप से अधिक अस्थिर हैं। परिणामस्वरूप, श्यान प्रत्यास्थ पॉइजुइल-कूएट प्रवाह को स्थिर करने के लिए दीवार का वेग न्यूटोनियन द्रव की तुलना में अधिक होना चाहिए। एसिम्प्टोटिक विश्लेषण का उपयोग करते हुए, हमने स्लिप लंबाई का महत्वपूर्ण मूल्य, या समकक्ष, निचली दीवार वेग का महत्वपूर्ण मूल्य निर्धारित किया है, जिसके ऊपर असममित स्लिप प्रवाह और श्यान प्रत्यास्थ द्रव का पॉइजुइल-कूएट प्रवाह अनंतिम छेड़छाड़ के लिए स्थायी रूप से स्थिर है।

Contents

Certificate

Acknowledgements

Abstract

Contents

List of Figures

List of Tables

Abbreviations

Symbols

1	Introduction	1
1.1	Hydrodynamic Stability	3
1.2	Literature Survey	4
1.3	Applications	10
1.4	Objectives	12
1.4.1	Objective 1: Linear stability of a surfactant-laden viscoelastic liquid flowing down a slippery inclined plane	12
1.4.2	Objective 2: Linear stability analysis of a contaminated shear-imposed viscoelastic liquid flowing down an inclined plane	12
1.4.3	Objective 3: Effect of imposed shear on the stability of a viscoelastic liquid flowing down a slippery plane	13
1.4.4	Objective 4: Role of slip in the stability of viscoelastic liquid flow through a channel	13
1.5	Organization of the Thesis	14
2	Methodologies	15

2.1	Introduction	15
2.2	Boundary Conditions	17
2.3	Orr-Sommerfeld Equation	19
2.4	Solution Procedures	21
2.4.1	Long-wave analysis	21
2.4.2	Padé approximation	21
2.4.3	Arbitrary wavenumber analysis	22
3	Linear stability of a surfactant-laden viscoelastic liquid flowing down a slippery inclined plane	25
3.1	Introduction	25
3.2	Mathematical Formulation	26
3.3	Orr-Sommerfeld Boundary Value Problem	30
3.4	Stability Analysis in the Long-wave Regime	32
3.4.1	Zeroth-order solution	33
3.4.2	First-order solution	35
3.4.3	Second-order solution	38
3.4.4	Third-order solution	40
3.5	Linear Stability Analysis for Arbitrary Wavenumber	42
3.5.1	Validation of the present numerical code	43
3.5.2	Effect of the viscoelastic coefficient on the primary instability	46
3.5.3	Effect of the slip length on the primary instability	49
3.5.4	Effect of the Marangoni number on the primary instability	52
4	Linear stability of a contaminated shear-imposed viscoelastic liquid flowing down an inclined plane	57
4.1	Introduction	57
4.2	Mathematical Formulation	58
4.3	Linearized Perturbation Equations	62
4.4	Orr-Sommerfeld Boundary Value Problem	64
4.4.1	Zeroth-order long-wave solution	66
4.4.2	First-order long-wave solution	67
4.5	Stability Analysis in the Moderate Reynolds Number Regime	71
4.5.1	Validation of the numerical code	73
4.5.2	Effect of the Weissenberg number on the surface mode	75
4.5.3	Effect of the Marangoni number on the surface mode	77
4.5.4	Effect of the imposed shear stress on the surface mode	79
4.6	Stability Analysis in the High Reynolds Number Regime	81
4.6.1	Effect of the Weissenberg number on the shear mode	82
4.6.2	Effect of the imposed shear stress on the shear mode	84
4.6.3	Effect of the Marangoni number on the shear mode	85
4.7	Comparison with the Results of Walters' Liquid B'' Model	86

4.8	Inertialess Stability Analysis	89
5	Effect of imposed shear on the stability of a viscoelastic liquid flowing down a slippery plane	91
5.1	Introduction	91
5.2	Mathematical Formulation	92
5.3	Orr-Sommerfeld Boundary Value Problem	96
5.4	Stability Analysis in the Long-wave Regime	99
5.4.1	Zeroth-order solution	100
5.4.2	First-order solution	101
5.5	Stability Analysis in the Moderate Reynolds Number Regime	106
5.5.1	Effect of the Weissenberg number on the surface mode	107
5.5.2	Effect of the slip length on the surface mode	110
5.5.3	Effect of the viscosity ratio on the surface mode	112
5.5.4	Effect of the interfacial shear stress on the surface mode	115
5.6	Stability Analysis in the High Reynolds Number Regime	118
5.6.1	Effect of the Weissenberg number on the shear mode	122
5.6.2	Effect of the slip length on the shear mode	123
5.6.3	Effect of the viscosity ratio on the shear mode	125
5.6.4	Effect of the imposed shear stress on the shear mode	126
5.7	Comparison Between Different Viscoelastic Liquids	129
5.8	Inertialess Stability Analysis	131
6	Role of slip in the stability of viscoelastic liquid flow through a channel	133
6.1	Introduction	133
6.2	Mathematical Formulation	134
6.2.1	Base flow solution	137
6.3	Orr-Sommerfeld Boundary Value Problem	137
6.3.1	Symmetric slip flow condition	139
6.3.2	Asymmetric slip flow condition	140
6.4	Numerical Solution of the Orr-Sommerfeld-type Equation	141
6.4.1	Comparison with the Poiseuille flow	145
6.4.2	Comparison with the Poiseuille-Couette flow	147
6.5	Results and Discussion	151
6.5.1	Asymmetric slip flow configuration	151
6.5.2	Symmetric slip flow configuration	153
6.5.3	Analogy to the Poiseuille-Couette flow configuration	154
6.6	Asymptotic Analysis	157
6.7	Effect of Maximum Shear Rate	161
7	Conclusion	163

7.1	Introduction	163
7.2	Summary of the Present Work	164
7.2.1	Linear stability of a surfactant-laden viscoelastic liquid flowing down a slippery inclined plane	164
7.2.2	Linear stability of a contaminated shear-imposed viscoelastic liquid flowing down an inclined plane	166
7.2.3	Effect of imposed shear on the stability of a viscoelastic liquid flowing down a slippery plane	168
7.2.4	Role of slip in the stability of viscoelastic liquid flow through a channel	169
7.3	Scope for Future Work	171
A Longwave Expressions		173
A.1	Solution of second-order long-wave equations	173
A.2	Expressions of the coefficients for third-order solution	176
B Surfactant Transport Equation		177
B.1	Derivation of the surfactant transport equation	177
C Validation		181
C.1	Validation of the numerical code	181
Bibliography		187
Author Bio-Data		201
List of Publications		203

List of Figures

1.1	Propagation of surface waves in a water surface [1].	2
1.2	(a) Conceptual model of surfactant dispersal into diseased lungs [2] (b) Progression of liquid plug through a symmetric airway network [3].	11
2.1	Sketch of a viscoelastic liquid (Oldroyd-B model) flowing down an inclined plane.	16
2.2	Free surface of a viscoelastic liquid flow.	18
2.3	(a) Variation of the neutral stability curve in (Re, k) plane for the surface mode. (b) Variation of the temporal growth rate kc_i with wavenumber k for the surface mode when $Re = 3$. The other flow parameter values are $\theta = 15^\circ$, $Wi = 5$, $S = 0.75$, and $Ca = 1/6$	23
3.1	Sketch of a surfactant-laden viscoelastic liquid (Walters' liquid B'') flowing down a slippery inclined plane.	27
3.2	Variation of the critical Reynolds number Re_{cs} for the surface mode with the viscoelastic coefficient M for different values of β when $Ma = 1$, $Ca = 2$, and $\theta = \pi/4$. Solid, dashed, and dotted lines stand for $\beta = 0$, $\beta = 0.04$, and $\beta = 0.08$, respectively. The points are results of the Bhat and Samanta [4].	33
3.3	(a) Variation of the phase speed c_r with wavenumber k for the surface mode. (b) Variation of the spatial growth rate $-k_i$ with wavenumber k_r for the surface mode. The other parameter values are $\theta = 4.6^\circ$, $Re = 23$, $Ma = 0$, $Ca = 0.008$, $M = 0$, and $\beta = 0$. The plus points are the experimental results of Liu <i>et al.</i> [5]. The solid points are the numerical results of Malamataris <i>et al.</i> [6].	42
3.4	(a) Variation of the neutral curve in (Re, k) plane for the shear mode when $\theta = 3'$.(b) Variation of the temporal growth rate kc_i with wavenumber k for the shear mode when $\theta = 3'$ and $Re = 5000$. The solid points are the results of Bruin [7]. The other parameter values are $Ma = 0$, $Ca = \infty$, $M = 0$, and $\beta = 0$. Here "U" and "S" specify the unstable and stable regions.	43

3.5	(a) Variation of the phase speed c_r with wavenumber k for the surface mode when $Re = 1.9$. (b) Variation of the temporal growth rate kc_i with wavenumber k for the surface mode when $Re = 1.9$. (c) Variation of the phase speed c_r with wavenumber k for the surface mode when $Re = 2$. (d) Variation of the temporal growth rate kc_i with wavenumber k for the surface mode when $Re = 2$. Solid, dashed, dotted and dash-dotted lines stand for numerical result, Padé approximation result, third-order long-wave result, and fifth-order long-wave result, respectively. The other parameter values are $\theta = 45^\circ$, $Ma = 1$, $M = 0.1$, $Ca = 2$, and $\beta = 0.04$	45
3.6	Variation of the neutral curve in (Re, k) plane for the surface mode when the viscoelastic coefficient M changes. Solid, dashed, and dotted lines stand for $M = 0$, $M = 0.01$, and $M = 0.02$, respectively. The other parameter values are $Ma = 1$, $Ca = 2$, $\theta = 4^\circ$, and $\beta = 0.04$. “U” and “S” represent unstable and stable regions. Points are the results computed from the expression of critical Reynolds number (3.45) obtained from the long-wave analysis. The stabilizing effect of the viscoelastic coefficient is shown in the inset of figure 3.6.	46
3.7	(a) Variation of the temporal growth rate kc_i with wavenumber k for the surface mode when $Re = 20$. (b) Variation of the temporal growth rate kc_i with wavenumber k for the surface mode when $Re = 30$. (c) Variation of the spatial growth rate $-k_i$ with wavenumber k_r for the surface mode when $Re = 20$. (d) Variation of the spatial growth rate $-k_i$ with wavenumber k_r for the surface mode when $Re = 30$. Solid, dashed, and dotted lines stand for $M = 0$, $M = 0.01$, and $M = 0.02$, respectively. The other parameter values are $Ma = 1$, $Ca = 2$, $\theta = 4^\circ$, and $\beta = 0.04$	47
3.8	(a) Variation of the neutral curve in (Re, k) plane for the shear mode when $\theta = 1^\circ$.(b) Variation of the temporal growth rate kc_i with wavenumber k for the shear mode when $\theta = 1^\circ$ and $Re = 13000$. Solid, dashed, and dotted lines stand for $M = 0$, $M = 0.0001$, and $M = 0.0003$, respectively. Solid points are the results of Bhat and Samanta [4]. The other parameter values are $Ma = 0$, $Ca = 0.034$, and $\beta = 0.02$. Here “U” and “S” specify the unstable and stable regions.	49
3.9	Variation of the neutral curve in (Re, k) plane for the surface mode when the slip length β changes. Solid, dashed, and dotted lines stand for $\beta = 0$, $\beta = 0.04$, and $\beta = 0.08$, respectively. The other parameter values are $Ma = 1$, $Ca = 2$, $\theta = 4^\circ$, and $M = 0.1$. “U” and “S” represent unstable and stable regions. Points are the results computed from the expression of critical Reynolds number (3.45) obtained from the long-wave analysis.	50

3.10	(a) Variation of the temporal growth rate kc_i with wavenumber k for the surface mode when $Re = 17$. (b) Variation of the temporal growth rate kc_i with wavenumber k for the surface mode when $Re = 30$. (c) Variation of the spatial growth rate $-k_i$ with wavenumber k_r for the surface mode when $Re = 17$. (d) Variation of the spatial growth rate $-k_i$ with wavenumber k_r for the surface mode when $Re = 30$. Solid, dashed, and dotted lines stand for $\beta = 0$, $\beta = 0.04$, and $\beta = 0.08$, respectively. The other parameter values are $Ma = 1$, $Ca = 2$, $\theta = 4^\circ$, and $M = 0.1$	51
3.11	(a) Variation of the neutral curve in (Re, k) plane for the shear mode when $\theta = 1^\circ$.(b) Variation of the temporal growth rate kc_i with wavenumber k for the shear mode when $\theta = 1^\circ$ and $Re = 23000$. Solid, dashed, and dotted lines stand for $\beta = 0$, $\beta = 0.02$, and $\beta = 0.04$, respectively. The other parameter values are $Ma = 0$, $Ca = 0.034$, and $M = 0.0001$. Here “U” and “S” specify the unstable and stable regions.	52
3.12	Variation of the neutral curve in (Re, k) plane for the surface mode when the Marangoni number Ma changes. Solid, dashed, and dotted lines stand for $Ma = 0$, $Ma = 1$, and $Ma = 2$, respectively. (a) $M = 0$ and (b) $M = 0.1$. The other parameter values are $Ca = 2$, $\theta = 4^\circ$, and $\beta = 0.04$. “U” and “S” represent unstable and stable regions. Points are the results computed from the expression of critical Reynolds number (3.45) obtained from the long-wave analysis.	53
3.13	(a) Variation of the temporal growth rate kc_i with wavenumber k for the surface mode when $Re = 20$. (b) Variation of the spatial growth rate $-k_i$ with wavenumber k_r for the surface mode when $Re = 20$. Solid, dashed, and dotted lines stand for $Ma = 0$, $Ma = 1$, and $Ma = 2$, respectively. The other parameter values are $M = 0.1$, $Ca = 2$, $\theta = 4^\circ$, and $\beta = 0.04$	53
3.14	(a) Variation of the neutral curve for the shear mode in (Re, k) plane when $\theta = 1'$.(b) Variation of the temporal growth rate kc_i with wavenumber k for the shear mode when $\theta = 1'$ and $Re = 15000$. Solid, dashed, and dotted lines stand for $Ma = 0$, $Ma = 0.5$, and $Ma = 1$, respectively. The other parameter values are $M = 0.0001$, $Ca = 0.00911$, and $\beta = 0.02$. Here “U” and “S” specify the unstable and stable regions.	54
4.1	Sketch of a surfactant-laden viscoelastic liquid flowing down an inclined plane when an interfacial shear stress is applied at the air-liquid interface.	59

4.2	(a) Variation of the spatial growth rate $-k_i$ with angular frequency ω for the surface mode when $Re = 0$ and the wavenumber k is complex. The solid points are the results of Shaqfeh <i>et al.</i> [8]. (b) Variation of the neutral stability curve in (Re, k) plane for the surface mode when the Weissenberg number Wi changes. Here the wavenumber k is real. Solid, dashed, and dotted lines stand for $Wi = 1$, $Wi = 0.5$, and $Wi = 0.1$, respectively. The other flow parameter values are $\theta = 90^\circ$, $Ma = 0$, $Ca = 1/6$, and $\tau = 0$. Here “U” and “S” specify the unstable and stable regions, respectively.	72
4.3	(a) Variation of the temporal growth rate kc_i with wavenumber k for the shear mode when $Re = 8000$. (b) Variation of the neutral stability curve in (Re, k) plane for the shear mode when $Wi = 0$, $\theta = 4^\circ$, $Ma = 0.5$, $Ca = 2$, and $\tau = 0.5$. Solid line represents the result obtained from the present numerical code while solid points are the results of Bhat and Samanta [9]. Here “U” and “S” specify the unstable and stable regions, respectively.	72
4.4	(a) Variation of the neutral stability curve in (Re, k) plane for the surface mode when the Weissenberg number Wi changes. (b) Variation of the temporal growth rate kc_i with wavenumber k for the surface mode when $Re = 25$. Solid, dashed, and dotted lines stand for $Wi = 0$, $Wi = 0.5$, and $Wi = 1$, respectively. The solid points are the values of the critical Reynolds number computed from the analytical expression (4.53). The other flow parameters values are $\theta = 4^\circ$, $Ma = 1$, $Ca = 1/6$, and $\tau = 0.4$. Here “U” and “S” specify the unstable and stable regions, respectively.	73
4.5	(a) Variation of the neutral stability curve in (Re, k) plane for the surface mode when the Marangoni number Ma changes. (b) Variation of the temporal growth rate kc_i with wavenumber k for the surface mode when $Re = 25$. Solid, dashed, and dotted lines stand for $Ma = 0$, $Ma = 0.5$, and $Ma = 1$, respectively. The solid points are the values of the critical Reynolds number computed from the analytical expression (4.53). The other flow parameters values are $\theta = 4^\circ$, $Wi = 1$, $Ca = 1/6$, and $\tau = 0.4$. Here “U” and “S” specify the unstable and stable regions, respectively.	76
4.6	(a) Variation of the neutral stability curve in (Re, k) plane for the surface mode when the interfacial shear stress τ changes. (b) Variation of the temporal growth rate kc_i with wavenumber k for the surface mode when $Re = 25$. Solid, dashed, and dotted lines stand for $\tau = 0$, $\tau = 0.2$, and $\tau = 0.4$, respectively. The solid points are the values of the critical Reynolds number computed from the analytical expression (4.53). The other flow parameters values are $\theta = 4^\circ$, $Wi = 1$, $Ca = 1/6$, and $Ma = 1$. Here “U” and “S” specify the unstable and stable regions, respectively.	76

4.7	(a) Eigenvalue spectrum of the characteristic polynomial (4.57) when $Re = 2500$, $k = 1.1$, $\theta = 4^\circ$, $\tau = 0.4$, $Ma = 1$, and $Ca = 1/6$. Here circle, square, and star points denote the results for $Wi = 0.5$, $Wi = 0.75$, and $Wi = 1$, respectively. (b) Eigenvalue spectrum of the characteristic polynomial (4.57) when $Re = 4500$, $k = 1.1$, $\theta = 4^\circ$, $Wi = 1$, $Ma = 1$, and $Ca = 1/6$. Here circle, square, and star points denote the results for $\tau = 0$, $\tau = 0.2$, and $\tau = 0.4$, respectively. (c) Eigenvalue spectrum of the characteristic polynomial (4.57) when $Re = 2500$, $k = 2$, $\theta = 1'$, $\tau = 1$, $Wi = 0.01$, and $Ca = 1/6$. Here circle, square, and star points denote the results for $Ma = 0$, $Ma = 10$, and $Ma = 20$, respectively. (d) Variation of the absolute value of the normalized eigenfunction $ \phi $ as a function of y when $Re = 2500$, $k = 2$, $\theta = 1'$, $\tau = 1$, $Wi = 0.01$, $Ca = 1/6$, and $Ma = 0$. The solid and dashed lines represent the eigenfunctions corresponding to the shear mode and surface mode, respectively.	80
4.8	(a) Variation of the neutral stability curve in (Re, k) plane for the shear mode when the Weissenberg number Wi changes. (b) Variation of the temporal growth rate kc_i with wavenumber k for the shear mode when $Re = 2500$. Solid, dashed, and dotted lines stand for $Wi = 0.5$, $Wi = 0.75$, and $Wi = 1$, respectively. The other flow parameter values are $\theta = 4^\circ$, $\tau = 0.4$, $Ma = 1$, and $Ca = 1/6$. Here “U” and “S” specify the unstable and stable regions, respectively.	83
4.9	(a) Variation of the neutral stability curve in (Re, k) plane for the shear mode when the interfacial shear stress τ changes. (b) Variation of the temporal growth rate kc_i with wavenumber k for the shear mode when $Re = 4500$. Solid, dashed, and dotted lines stand for $\tau = 0$, $\tau = 0.2$, and $\tau = 0.4$, respectively. The other flow parameter values are $\theta = 4^\circ$, $Wi = 1$, $Ma = 1$, and $Ca = 1/6$. Here “U” and “S” specify the unstable and stable regions, respectively.	83
4.10	(a) Variation of the neutral stability curve in (Re, k) plane for the shear mode when the Marangoni number Ma changes. (b) Variation of the temporal growth rate kc_i with wavenumber k for the shear mode when $Re = 2500$. Solid, dashed, and dotted lines stand for $Ma = 0$, $Ma = 10$, and $Ma = 20$, respectively. The other flow parameter values are $\theta = 1'$, $Wi = 0.01$, $Ca = 1/6$, and $\tau = 1$. Here “U” and “S” specify the unstable and stable regions, respectively.	84

4.11	(a) Variation of the neutral stability curve in (Re, k) plane for the surface mode when the viscoelastic parameter M of Walters' liquid B'' model and the Weissenberg number Wi of UCM model vary. (b) Variation of the temporal growth rate kc_i with wavenumber k for the surface mode when $Re = 20$. The thin and thick solid, dashed, and dotted lines represent $M = 0.01$, $M = 0.05$, and $M = 0.1$ and corresponding $Wi = 0.056$, $Wi = 0.280$, and $Wi = 0.56$, respectively. The other flow parameter values are $\theta = 15^\circ$, $Ma = 0.5$, and $Ca = 1/6$. Here "U" and "S" specify the unstable and stable regions, respectively.	86
4.12	(a) Variation of the phase speed c_r with wavenumber k when $Re \rightarrow 0$. (b) Variation of the temporal growth rate kc_i with wavenumber k when $Re \rightarrow 0$. Solid, dashed, and dotted lines stand for $Wi = 1$, $Wi = 0.5$, and $Wi = 0.1$, respectively. The other flow parameter values are $\theta = 45^\circ$, $Ma = 0$, $Ca = 1/6$, and $\tau = 0$. Here thick lines and thin lines specify the numerical and long-wave analytical results, respectively.	87
5.1	A sketch of a shear-imposed viscoelastic Oldroyd-B liquid draining down a slippery inclined plane.	92
5.2	(a) Variation of the critical Reynolds number for the surface mode when the slip length β changes, and $\tau = 0.4$ and $\theta = 4^\circ$. (b) Variation of the critical Reynolds number for the surface mode when the imposed shear stress τ changes, and $\beta = 0.04$ and $\theta = 4^\circ$. Solid, dashed, and dotted lines represent the results for the Oldroyd-B liquid ($S = 0.75$ and $Wi = 1$), upper-convected Maxwell liquid ($S = 0$ and $Wi = 1$), and Newtonian liquid ($S = 1$ and $Wi = 0$), respectively. (c) Variation of the critical Reynolds number for the Oldroyd-B liquid corresponding to the surface mode when the imposed shear stress τ varies and $\beta = 0.04$, $S = 0.75$, $Wi = 1$, and $\theta = 90^\circ$. The other flow parameter value is $Ca = 1/6$.	104
5.3	(a) Variation of the critical Weissenberg number Wi_c with viscosity ratio S when $\beta = 0.04$. Here, Wi_c is computed by using equation (5.36) for the inertialess flow configuration ($Re = 0$). Solid, dashed, and dotted lines stand for $\tau = 0.1$, $\tau = 0$, and $\tau = -0.1$, respectively. (b) Variation of the critical Weissenberg number Wi_c with viscosity ratio S when $\tau = 0.4$. Solid, dashed, and dotted lines stand for $\beta = 0.08$, $\beta = 0.04$, and $\beta = 0$, respectively. The other flow parameter values are $\theta = 4^\circ$ and $Ca = 1/6$.	106

5.4	Variation of the neutral stability curve in (Re, k) plane for the surface mode when the Weissenberg number Wi changes. Solid, dashed, and dotted lines stand for $Wi = 3$, $Wi = 2$, and $Wi = 1$, respectively. The solid points are the values of the critical Reynolds number computed from the analytical expression (5.35). The other flow parameter values are $\theta = 4^\circ$, $\beta = 0.02$, $S = 0.75$, $Ca = 1/6$, and $\tau = 0.4$. Here “U” and “S” specify the unstable and stable regions, respectively.	108
5.5	(a) Variation of the temporal growth rate kc_i with wavenumber k for the surface mode when $Re = 18$. k is real for the temporal growth rate. (b) Variation of the spatial growth rate $-k_i$ with wavenumber k_r for the surface mode when $Re = 18$. $k = k_r + ik_i$ is complex for the spatial growth rate. Solid, dashed, and dotted lines stand for $Wi = 3$, $Wi = 2$, and $Wi = 1$, respectively. The other flow parameter values are $\theta = 4^\circ$, $\beta = 0.02$, $S = 0.75$, $Ca = 1/6$, and $\tau = 0.4$	109
5.6	Variation of the neutral stability curve in (Re, k) plane for the surface mode when the slip length β changes. Solid, dashed, and dotted lines stand for $\beta = 0.08$, $\beta = 0.04$, and $\beta = 0$, respectively. The solid points are the values of the critical Reynolds number computed from the analytical expression (5.35). The other flow parameter values are $\theta = 4^\circ$, $Wi = 1$, $S = 0.75$, $Ca = 1/6$, and $\tau = 0.4$. Here “U” and “S” specify the unstable and stable regions, respectively.	110
5.7	(a) Variation of the temporal growth rate kc_i with wavenumber k for the surface mode when $Re = 25$. k is real for the temporal growth rate. (b) Variation of the spatial growth rate $-k_i$ with wavenumber k_r for the surface mode when $Re = 25$. $k = k_r + ik_i$ is complex for the spatial growth rate. Solid, dashed, and dotted lines stand for $\beta = 0.08$, $\beta = 0.04$, and $\beta = 0$, respectively. The other flow parameter values are $\theta = 4^\circ$, $Wi = 1$, $S = 0.75$, $Ca = 1/6$, and $\tau = 0.4$	111
5.8	Variation of the neutral stability curve in (Re, k) plane for the surface mode when the viscosity ratio S changes. Solid, dashed, dotted, and dash-dotted lines stand for $S = 0.75$, $S = 0.5$, $S = 0.25$, and $S = 0$, respectively. The solid points are the values of the critical Reynolds number computed from the analytical expression (5.35). The other flow parameter values are $\theta = 4^\circ$, $Wi = 1$, $\beta = 0.02$, $Ca = 1/6$, and $\tau = 0.4$. Here “U” and “S” specify the unstable and stable regions, respectively.	112

- 5.9 (a) Variation of the temporal growth rate kc_i with wavenumber k for the surface mode when $Re = 14$. (b) Variation of the temporal growth rate kc_i with wavenumber k for the surface mode when $Re = 18$. k is real for the temporal growth rate. (c) Variation of the spatial growth rate $-k_i$ with wavenumber k_r for the surface mode when $Re = 14$. (d) Variation of the spatial growth rate $-k_i$ with wavenumber k_r for the surface mode when $Re = 18$. $k = k_r + ik_i$ is complex for the spatial growth rate. Solid, dashed, dotted, and dash-dotted lines stand for $S = 0.75$, $S = 0.5$, $S = 0.25$, and $S = 0$, respectively. The other flow parameter values are $\theta = 4^\circ$, $Wi = 1$, $\beta = 0.02$, $Ca = 1/6$, and $\tau = 0.4$. 114
- 5.10 (a) Variation of the neutral stability curve in (Re, k) plane for the surface mode when the imposed shear stress τ acts in the co-flow direction. Solid, dashed, and dotted lines stand for $\tau = 0.4$, $\tau = 0.2$, and $\tau = 0$, respectively. (b) Variation of the neutral stability curve in (Re, k) plane for the surface mode when the imposed shear stress τ acts in the counter-flow direction. Solid, dashed, and dotted lines stand for $\tau = -0.6$, $\tau = -0.4$, and $\tau = -0.2$, respectively. The solid points are the values of the critical Reynolds number computed from the analytical expression (5.35). The other flow parameter values are $\theta = 4^\circ$, $Wi = 1$, $\beta = 0.02$, $S = 0.75$, and $Ca = 1/6$. Here “U” and “S” specify the unstable and stable regions, respectively. 116
- 5.11 (a) Variation of the temporal growth rate kc_i with wavenumber k for the surface mode when $Re = 25$. k is real for the temporal growth rate. (b) Variation of the spatial growth rate $-k_i$ with wavenumber k_r for the surface mode when $Re = 25$. k is complex for the spatial growth rate. Solid, dashed, and dotted lines stand for $\tau = 0.4$, $\tau = 0.2$, and $\tau = 0$, respectively. (c) Variation of the temporal growth rate kc_i with wavenumber k for the surface mode when $Re = 28$. k is real for the temporal growth rate. (d) Variation of the spatial growth rate $-k_i$ with wavenumber k_r for the surface mode when $Re = 28$. k is complex for the spatial growth rate. Solid, dashed, and dotted lines stand for $\tau = -0.6$, $\tau = -0.4$, and $\tau = -0.2$, respectively. The other flow parameter values are $\theta = 4^\circ$, $Wi = 1$, $\beta = 0.02$, $S = 0.75$, and $Ca = 1/6$ 117

5.12	(a) Eigenvalue spectrum of the characteristic polynomial (5.39) when $Re = 7500$, $k = 0.9$, $\theta = 4^\circ$, $\tau = 0.4$, $\beta = 0.02$, $S = 0.75$, and $Ca = 1/6$. Here, circle, square, and star points denote the results for $Wi = 0.5$, $Wi = 1$, and $Wi = 1.5$, respectively. (b) Eigenvalue spectrum of the characteristic polynomial (5.39) when $Re = 7000$, $k = 1$, $\theta = 4^\circ$, $Wi = 1$, $\tau = 0.4$, $S = 0.75$, and $Ca = 1/6$. Here, circle, square, and star points denote the results for $\beta = 0$, $\beta = 0.02$, and $\beta = 0.04$, respectively. (c) Eigenvalue spectrum of the characteristic polynomial (5.39) when $Re = 15000$, $k = 0.8$, $\theta = 4^\circ$, $Wi = 1$, $\tau = 0.4$, $\beta = 0.02$, and $Ca = 1/6$. Here, circle, square, and star points denote the results for $S = 0.25$, $S = 0.5$, and $S = 0.75$, respectively. (d) Eigenvalue spectrum of the characteristic polynomial (5.39) when $Re = 14000$, $k = 0.85$, $\theta = 4^\circ$, $Wi = 1$, $\beta = 0.02$, $S = 0.75$, and $Ca = 1/6$. Here diamond, cross, circle, square, and star points denote the results for $\tau = -0.4$, $\tau = -0.2$, $\tau = 0$, $\tau = 0.2$, and $\tau = 0.4$, respectively.	119
5.13	Variation of the absolute value of normalized eigenfunction $ \phi $ as a function of y when $Re = 6500$, $k = 1$, $\theta = 4^\circ$, $Wi = 1$, $\tau = 0.4$, $\beta = 0.02$, $S = 0.75$ and $Ca = 1/6$. The solid and dashed lines represent the eigenfunctions corresponding to the shear mode and surface mode, respectively.	120
5.14	(a) Variation of the neutral stability curve in (Re, k) plane for the shear mode when the Weissenberg number Wi changes. (b) Variation of the temporal growth rate kc_i with wavenumber k for the shear mode when $Re = 8000$. Solid, dashed, and dotted lines stand for $Wi = 1.5$, $Wi = 1$, and $Wi = 0.5$, respectively. The other flow parameter values are $\theta = 4^\circ$, $\beta = 0.02$, $S = 0.75$, $Ca = 1/6$, and $\tau = 0.4$. Here “U” and “S” specify the unstable and stable regions, respectively.	122
5.15	(a) Variation of the neutral stability curve in (Re, k) plane for the shear mode when the slip length β changes. (b) Variation of the temporal growth rate kc_i with wavenumber k for the shear mode when $Re = 14000$. Solid, dashed, and dotted lines stand for $\beta = 0.04$, $\beta = 0.02$, and $\beta = 0$, respectively. The other flow parameter values are $\theta = 4^\circ$, $Wi = 1$, $S = 0.75$, $Ca = 1/6$, and $\tau = 0.4$. Here “U” and “S” specify the unstable and stable regions, respectively.	124
5.16	(a) Variation of the neutral stability curve in (Re, k) plane for the shear mode when the viscosity ratio S changes. (b) Variation of the temporal growth rate kc_i with wavenumber k for the shear mode when $Re = 8000$. Solid, dashed, dotted, and dash-dotted lines stand for $S = 0.75$, $S = 0.5$, $S = 0.25$, and $S = 0$, respectively. The other flow parameter values are $\theta = 4^\circ$, $Wi = 1$, $\beta = 0.02$, $Ca = 1/6$, and $\tau = 0.4$. Here “U” and “S” specify the unstable and stable regions, respectively.	125

5.17	(a) Variation of the neutral stability curve in (Re, k) plane for the shear mode when the imposed shear stress $\tau \geq 0$ changes. (b) Variation of the temporal growth rate kc_i with wavenumber k for the shear mode when $Re = 12000$. Solid, dashed, and dotted lines stand for $\tau = 0.4$, $\tau = 0.2$, and $\tau = 0$, respectively. (c) Variation of the neutral stability curve in (Re, k) plane for the shear mode when the imposed shear stress $\tau \leq 0$ changes. (d) Variation of the temporal growth rate kc_i with wavenumber k for the shear mode when $Re = 12000$. Solid, dashed, and dotted lines stand for $\tau = -0.1$, $\tau = -0.05$, and $\tau = 0$, respectively. The other flow parameter values are $\theta = 4^\circ$, $Wi = 1$, $\beta = 0.02$, $S = 0.75$, and $Ca = 1/6$. Here “U” and “S” specify the unstable and stable regions, respectively.	127
5.18	(a) Variation of the neutral stability curve in (Re, k) plane for the surface mode when the viscoelastic parameter M of Walters’ liquid B'' and the Weissenberg number Wi of Oldroyd-B liquid alter. (b) Variation of the temporal growth rate kc_i with wavenumber k for the surface mode when $Re = 18$. Thick solid, thick dashed, and thick dotted lines are the results corresponding to the Oldroyd-B liquid for $Wi = 0.71$, $Wi = 1.43$, and $Wi = 2.14$, respectively. Thin solid, thin dashed, and thin dotted lines are the results corresponding to Walters’ liquid B'' for $M = 0.01$, $M = 0.02$, and $M = 0.03$, respectively. The other flow parameter values are $\theta = 4^\circ$, $Ca = 1/6$, and $S = 0.75$. Here “U” and “S” specify the unstable and stable regions, respectively.	128
5.19	(a) Variation of the temporal growth rate kc_i with wavenumber k when the Weissenberg number changes and $\tau = 0$. Solid, dashed, and dotted lines stand for $Wi = 1.5$, $Wi = 1.0$, and $Wi = 0.5$, respectively. (b) Variation of the temporal growth rate kc_i with wavenumber k when the imposed shear stress τ changes and $Wi = 1$. Solid, dashed, dotted, and dash-dotted lines stand for $\tau = -0.8$, $\tau = -0.6914$, $\tau = -0.3$, and $\tau = 0$, respectively. The other flow parameters are $Re = 0$, $\theta = 90^\circ$, $S = 0.75$, $Ca = 1/6$, and $\beta = 0.04$	131
6.1	Sketch of a viscoelastic Walters’ liquid B'' flowing through a slippery channel.	136
6.2	The spectrum of the eigenvalue problem (6.19) for the symmetric slip flow when the viscoelastic parameter M varies $M \in [0, 0.0002]$. Here, $Re = 10000$, $k = 1$, and $\beta = 0.01$. The circles represent the result for $M = 0$, while the dot points represent the spectrum with increasing M . The variation of the most unstable shear mode with M is shown in the inset of Fig. 6.2.	142

6.3	(a)	Variation of the neutral stability curve corresponding to the shear mode for the Poiseuille flow of the viscoelastic Walters' liquid B'' in (Re, k) plane for different values of M when $\beta_1 = \beta_2 = 0$. Small circles are the results of Porteous and Denn [10]. (b) Variation of the neutral stability curve corresponding to the shear mode for the symmetric slip flow of the Newtonian liquid in (Re, k) plane for different values of β ($\beta_1 = \beta_2 = \beta$) when $M = 0$. (c) Absolute value of the normalized eigenfunction $ \phi $ corresponding to the shear mode is computed at the critical point (Re_c, k_c) for the symmetric slip flow of the Newtonian liquid when $M = 0$. Small circles in both Figs. 6.3(b) and 6.3(c) are the results of Ceccacci <i>et al.</i> [11]. Here "U" and "S" specify the unstable and stable regions.	143
6.4	(a)	Variation of the neutral stability curves corresponding to the shear mode for the asymmetric slip flow and the Poiseuille-Couette flow of the Newtonian liquid in (Re, k) plane for different values of $\beta_1 = \beta$ when $M = 0$ and $\beta_2 = 0$. (b) Absolute value of the normalized eigenfunction $ \phi $ corresponding to the shear mode is computed at the critical point (Re_c, k_c) given in Table 6.2 for the Newtonian liquid when $M = 0$ and $\beta_2 = 0$. Small circles in both Figs. 6.4(a) and 6.4(b) are the results of Ceccacci <i>et al.</i> [11]. (c) Variation of the neutral stability curves corresponding to the shear mode for the asymmetric slip flow and the Poiseuille-Couette flow of the viscoelastic Walters' liquid B'' in (Re, k) plane for different values of $\beta_1 = \beta$ when $M = 5 \times 10^{-5}$ and $\beta_2 = 0$. Thick and thin lines stand for the results of the asymmetric slip flow and the Poiseuille-Couette flow, respectively. Here "U" and "S" specify the unstable and stable regions.	144
6.5	(a)	Variation of the neutral stability curve corresponding to the shear mode for the asymmetric slip flow of Walters' liquid B'' in (Re, k) plane for different values of M when $\beta_1 = 0.01$ ($\beta_1 = \beta$) and $\beta_2 = 0$. (b) Variation of the neutral stability curve corresponding to the shear mode for the asymmetric slip flow of Walters' liquid B'' in (Re, k) plane for different values of β_1 ($\beta_1 = \beta$) when $M = 5 \times 10^{-5}$ and $\beta_2 = 0$. (c) Variation of the neutral stability curve corresponding to the shear mode for the asymmetric slip flow of Walters' liquid B'' in (Re, k) plane for different values of β_2 when $M = 5 \times 10^{-5}$ and $\beta_1 = 0.2$. Thin solid lines in Figs. 6.5(b) and 6.5(c) indicate the variation of Re_c for the onset of the shear mode instability. Here "U" and "S" specify the unstable and stable regions.	147

6.6	(a) Variation of the neutral stability curve corresponding to the shear mode for the symmetric slip flow of Walters' liquid B'' in (Re, k) plane for different values of M when $\beta = 0.01$ ($\beta_1 = \beta_2 = \beta$). (b) Variation of the neutral stability curve corresponding to the shear mode for the symmetric slip flow of Walters' liquid B'' in (Re, k) plane for different values of β ($\beta_1 = \beta_2 = \beta$) when $M = 5 \times 10^{-5}$. (c) Variation of the neutral stability curve corresponding to the shear mode for the slip flow of Walters' liquid B'' in (Re, k) plane for different values of β when $M = 5 \times 10^{-5}$. Thin and thick lines stand for the results corresponding to the symmetric slip flow ($\beta_2 = \beta_1 = \beta$) and the asymmetric slip flow ($\beta_1 = \beta, \beta_2 = 0$), respectively. Here "U" and "S" specify the unstable and stable regions.	150
6.7	(a) Variation of the temporal growth rate corresponding to the shear mode for the symmetric slip flow of Walters' liquid B'' for different values of M when $\beta = 0.01$ ($\beta_1 = \beta_2 = \beta$) and $Re = 8000$. (b) Variation of the temporal growth rate corresponding to the shear mode for the symmetric slip flow of Walters' liquid B'' for different values of β ($\beta_1 = \beta_2 = \beta$) when $M = 5 \times 10^{-5}$ and $Re = 18000$. (c) Variation of the temporal growth rate corresponding to the shear mode for the slip flow of Walters' liquid B'' for different values of β when $M = 5 \times 10^{-5}$ and $Re = 18000$. Thin and thick lines stand for the results corresponding to the symmetric slip flow ($\beta_2 = \beta_1 = \beta$) and the asymmetric slip flow ($\beta_1 = \beta, \beta_2 = 0$), respectively.	152
6.8	(a) Variation of the neutral stability curve corresponding to the shear mode for the slip flow similar to the Poiseuille-Couette flow configuration in (Re, k) plane for different values of M when $\beta_1 = 0.01$ ($\beta_1 = \beta$) and $\beta_2 = 0$. (b) Variation of the neutral stability curve corresponding to the shear mode for the slip flow similar to the Poiseuille-Couette flow configuration in (Re, k) plane for different values of β_1 ($\beta_1 = \beta$) when $M = 5 \times 10^{-5}$ and $\beta_2 = 0$. (c) Variation of the critical slip length $\beta_{1c} = \beta_c$ and the critical wall velocity W_c with the viscoelastic parameter M . Square points are the results of Ceccacci <i>et al.</i> [11] and Potter [12] when $M = 0$. Star points are the present results corresponding to Walters' liquid B'' . Here "U" and "S" specify the unstable and stable regions.	155

6.9	(a) Variation of the scaled wavelength γ with the slip length β_1 ($\beta = \beta_1$) corresponding to the asymmetric slip flow for different values of M when $\beta_2 = 0$. (b) Variation of the scaled wavelength γ with the slip length β_1 ($\beta = \beta_1$) corresponding to the Poiseuille-Couette flow for different values of M when $\beta_2 = 0$. (c) Variation of the scaled wavelength γ with the slip length β_1 ($\beta = \beta_1$) corresponding to the asymmetric slip flow for different values of β_2 when $M = 2.5 \times 10^{-5}$. The black circles are the results of Ceccacci <i>et al.</i> [11] for the Newtonian liquid, and the red squares are the cut-off/critical values of β_{1c} and γ_c given in Table 6.3 and Table 6.4. Here “U” and “S” specify the unstable and stable regions.	157
6.10	(a) Variation of the phase speed c_r with the slip length β_1 ($\beta_1 = \beta$) corresponding to the asymmetric slip flow for different values of M . (b) Variation of the phase speed c_r with the slip length β_1 ($\beta = \beta_1$) corresponding to the Poiseuille-Couette flow for different values of M . (c) Variation of the phase speed c_r with the slip length β_1 ($\beta_1 = \beta$) corresponding to the asymmetric slip flow for different values of β_2 when $M = 2.5 \times 10^{-5}$. The black circles are the results of Ceccacci <i>et al.</i> [11] for the Newtonian liquid, and the red squares are the cut-off/critical values of β_{1c} and c_{rc} given in Table 6.3 and Table 6.4. Here “U” and “S” specify the unstable and stable regions.	161
6.11	(a) Variation of the neutral stability curve corresponding to the shear mode for the symmetric slip flow of Walters’ liquid B'' in (Re, k) plane for different values of R_M when $\beta = 0.01$ ($\beta_1 = \beta_2 = \beta$). (b) Variation of the neutral stability curve corresponding to the shear mode for the asymmetric slip flow of Walters’ liquid B'' in (Re, k) plane for different values of R_M when $\beta_1 = 0.2$ and $\beta_2 = 0$. (c) Variation of the neutral stability curve corresponding to the shear mode for the Poiseuille-Couette flow of Walters’ liquid B'' in (Re, k) plane for different values of R_M when $\beta_1 = 0.2$ ($W = 0.364$). Here “U” and “S” specify the unstable and stable regions.	162
B.1	Schematic diagram of the transport of insoluble surfactant at the viscoelastic liquid surface in the time interval t to $t + \Delta t$	178
C.1	(a) Variation of the neutral stability curve in (Re, k) plane for the surface mode corresponding to the Newtonian liquid when $\theta = 4^\circ$, $Wi = 0$, $\beta = 0$, $S = 1$, $Ca = 0.5762$, and $\tau = 0$. The solid points are the results of Samanta <i>et al.</i> [13]. (b) Variation of the neutral stability curve in (Re, k) plane for the shear mode corresponding to the Newtonian liquid when $\theta = 1^\circ$, $Wi = 0$, $\beta = 0$, $S = 1$, $Ca = 0.034$, and $\tau = 0$. The solid points are the results of Chin <i>et al.</i> [14]. Here “U” and “S” specify the unstable and stable regions, respectively. . .	183

C.2 (a) Variation of the neutral stability curve in (Re, k) plane for the surface mode corresponding to the concentrated polymer solution when $\theta = 4^\circ$, $Wi = 1$, $\beta = 0$, $S = 0$, $Ca = 1/6$, and $\tau = 0.4$. The solid points are the results of Pal and Samanta [15]. (b) Variation of the neutral stability curve in (Re, k) plane for the shear mode corresponding to the concentrated polymer solution when $\theta = 4^\circ$, $Wi = 0.75$, $\beta = 0$, $S = 0$, $Ca = 1/6$, and $\tau = 0.4$. The solid points are the results of Pal and Samanta [15]. Here “U” and “S” specify the unstable and stable regions, respectively. 183

C.3 (a) Variation of the neutral stability curve in (Re, k) plane for the surface mode when the Weissenberg number Wi changes. Solid, dashed, dotted, and dash-dotted lines stand for $Wi = 5$, $Wi = 3$, $Wi = 1$, and $Wi = 0$, respectively. The other flow parameter values are $\theta = 90^\circ$, $\beta = 0$, $S = 0.75$, $Ca = 1/6$, and $\tau = 0$. Here “U” and “S” specify the unstable and stable regions, respectively. (b) Variation of the spatial growth rate $-k_i$ with angular frequency ω for the surface mode when $Re = 0$. Solid, dashed, and dotted lines stand for $Wi = 2.5$, $Wi = 2$, and $Wi = 1$, respectively. The other flow parameter values are $\theta = 90^\circ$, $\beta = 0$, $S = 0.75$, $Ca = 1/2400$, and $\tau = 0$. The solid points are the results of Shaqfeh *et al.* [8]. 184

List of Tables

3.1	Comparison between the analytical and numerical values of the critical Reynolds number Re_{cs} for the surface mode when the viscoelastic coefficient M varies. Here, $\theta = 45^\circ$, $Ma = 1$, $Ca = 2$, and $\beta = 0.04$. . .	44
4.1	Physical properties of the concentrated polymer solution	62
4.2	Comparison between the analytical and numerical values of the critical Reynolds number Re_c for the surface mode when the Weissenberg number Wi varies. Here $\theta = 15^\circ$, $Ma = 1$, $Ca = 1/6$, and $\tau = 0.4$. . .	69
4.3	Comparison between the analytical and numerical values of the critical Reynolds number Re_c for the surface mode when the Marangoni number Ma varies. Here $\theta = 15^\circ$, $Wi = 1$, $Ca = 1/6$, and $\tau = 0.1$. . .	69
4.4	Comparison between the analytical and numerical values of the critical Reynolds number Re_c for the surface mode when the interfacial shear stress τ varies. Here $\theta = 15^\circ$, $Wi = 1$, $Ca = 1/6$, and $Ma = 1$. . .	69
4.5	Comparison between the critical Reynolds number Re_c corresponding to the surface mode for Walters' liquid B'' model and upper-convected Maxwell model when the viscoelastic parameter M and the corresponding Wi vary. Here $\theta = 15^\circ$, $Ma = 0.5$, $Ca = 1/6$, and $\tau = 0$. . .	86
5.1	Range of various non-dimensional parameters for different polymer solutions [8]	99
5.2	Comparison of the critical Reynolds number between Walters' liquid B'' and Oldroyd-B liquid for the surface mode when the viscoelastic parameter M and the corresponding Weissenberg number Wi vary. Here $\theta = 4^\circ$ and $S = 0.75$	130
6.1	Values of the complex wave speed c corresponding to the most unstable shear mode for the symmetric slip flow (symmetric slip flow conditions are given by equations (6.14) and (6.15)) for different values of the number of Chebyshev polynomials N and for two different values of the viscoelastic parameter M when $Re = 8000$, $k = 1$, and $\beta = 0.01$ ($\beta_1 = \beta_2 = \beta$).	141

6.2	Variation of the critical Reynolds number and the critical wavenumber corresponding to the onset of the shear mode instability for the Poiseuille-Couette flow of the Newtonian liquid at different values of β_1 ($\beta_1 = \beta$) when $M = 0$ and $\beta_2 = 0$	146
6.3	Cut-off/critical values of β_{1c} , γ_c , and c_{rc} for different values of the viscoelastic parameter M corresponding to the asymmetric slip flow when $\beta_2 = 0$	159
6.4	Cut-off/critical values of β_{1c} , γ_c , W_c , and c_{rc} for different values of the viscoelastic parameter M corresponding to the Poiseuille-Couette flow when $\beta_2 = 0$	159
C.1	Comparison between the analytical and numerical values of the critical Reynolds number Re_c for the surface mode when the Weissenberg number Wi varies. Here $\theta = 15^\circ$, $\beta = 0.02$, $S = 0.75$, $Ca = 1/6$, and $\tau = 0.4$	182
C.2	Comparison between the analytical and numerical values of the critical Reynolds number Re_c for the surface mode when the slip length β varies. Here $\theta = 15^\circ$, $Wi = 1$, $S = 0.75$, $Ca = 1/6$, and $\tau = 0.4$	182
C.3	Comparison between the analytical and numerical values of the critical Reynolds number Re_c for the surface mode when the viscosity ratio S varies. Here $\theta = 15^\circ$, $Wi = 1$, $\beta = 0.02$, $Ca = 1/6$, and $\tau = 0.2$	182
C.4	Comparison between the analytical and numerical values of the critical Reynolds number Re_c for the surface mode when the imposed shear stress τ varies. Here $\theta = 15^\circ$, $Wi = 1$, $\beta = 0.02$, $S = 0.75$, and $Ca = 1/6$	184

Abbreviations

OSE	Orr-Sommerfeld E quations
OS BVP	Orr-Sommerfeld B oundary V alue P roblem
WB	W alters' liquid B " Model
UCM	U pper- C onvected M axwell Model
OB	O ldroyd- B Model

Symbols

c	Complex wave speed
d	Height of undisturbed film
Ca	Capillary number
D_s	Diffusivity of surfactant
g	Gravitational acceleration
h	Height of disturbed film
k	Wave-number
M	Viscoelastic parameter
Ma	Marangony number
p	Pressure field
Re	Reynolds number
Re_c	Critical Reynolds number
S	Viscosity ratio
t	Time
T_n	n^{th} degree Chebyshev polynomial of first kind
U	Base flow velocity
\mathbf{V}	Velocity vector
Wi	Weissenberg number
Wi_c	Critical Weissenberg number
α	Dimensional slip length
β	Non-dimensional slip length
γ	Non-dimensional amplitude of surfactant concentration
η	Non-dimensional amplitude of free surface deformation
λ	Wavelength of disturbance
μ	Total viscosity
μ_0	Dynamic viscosity

Symbols

μ_p	Polymeric viscosity
μ_s	Solvent viscosity
ρ	Density of fluid
σ	Surface tension
ψ	Non-dimensional stream function
ϕ	Non dimensional amplitude of stream-function
ω	Angular frequency
∂_x	Partial derivative with respect to x
Γ	Surfactant concentration
$\boldsymbol{\tau}$	Stress tensor
τ_s	Imposed shear stress
θ	Angle of inclination